



Preparation and characterization of conductive and transparent silver nanowire thin films

Michał Kamiński

University of Silesia, Institute of Physics, Poland

Supervisor: Dr. Wiebke Ohm

Hamburg, 5.09.2017.

Abstract

In this report, an investigation of spray deposition process of silver nanowire thin films, followed by characterization of obtained samples is presented. Particularly, samples' conductivity and transparency, as well as surface coverage studies were performed. These were complemented with grazing incidence small angle x-ray scattering measurements, since it is a proper method of investigating the structure of thin films.

Contents

1	Introduction	3
2	Theoretical background	3
2.1	Air-brush spray deposition	3
2.2	Grazing incidence small angle x-ray scattering	4
3	Experimental section	7
3.1	Sample preparation	7
3.2	Initial characterization	8
3.2.1	Conductivity measurements	8
3.2.2	Optical microscopy	8
3.2.3	Transmission measurements	10
3.3	Relations between properties and deposition parameters	12
3.3.1	Temperature of the substrate	13
3.3.2	Time of spraying	14
3.3.3	Time structure of the process	14
3.3.4	Nozzle-to-sample distance	15
3.3.5	Size of nanowires	15
3.3.6	Final remarks, set of optimal parameters	16
3.4	Atomic force microscopy	16
3.5	GISAXS measurements	18
3.5.1	General description	18
3.5.2	Alignment	18
3.5.3	Calibration	18
3.5.4	Results	20
3.5.5	Analysis of GISAXS data - fitting	22
4	Summary	27

1 Introduction

Thin layers are widely used in many branches of modern industry. They find an application in photovoltaics, particularly in production of solar cells. Optimization of the process of thin films preparation is of a significant importance for industry. That is therefore essential to investigate the process itself and to tailor the deposition parameters to the properties of obtained samples.

The main aim of this work was to prepare both conductive and transparent thin layers, which could be then used as electrodes for solar cells. Due to the first desired feature, namely conductivity, silver nanowires were chosen as a material for deposition.

Methods of deposition of thin films can be divided into two groups: solution-based and vacuum-based ones. Among the first group there is an air-brush spray coating, a method that is relatively easy to use and apart from application in science, can be also utilized for industrial purposes.

Initial investigation of samples' properties was performed by optical microscopy, UV-Vis spectroscopy and conductivity measurements. The first method was used to estimate the nanowire concentration on the substrate's surface, whereas UV-Vis spectroscopy to determine the transmission coefficient of thin layers. These three methods gave quantitative information about deposited films. Additionally, atomic force microscopy (AFM) was conducted to verify the results obtained by optical microscopy.

Final research of given structures was conducted with the use of grazing incidence small angle x-ray scattering (GISAXS) on the beamline P03 on synchrotron PETRA III. GISAXS is a proper method for the investigation of structure of thin films. Small incident angle of incoming beam with respect to sample's surface, which is a key feature of this method, leads to highly reduced penetration depth of x-rays in the sample, and therefore, to the increase of surface sensitivity. What is more, big sample-to-detector distance being used, reduces the obtained information only to small q values, consequently enabling to probe relatively big distances in the real space. In contrast to wide angle x-ray scattering (WAXS), which is an atomic-resolution method, from GISAXS results one can learn about the arrangement of whole structures, like nanoparticles or nanowires, as well as about their size and shape.

2 Theoretical background

2.1 Air-brush spray deposition

Spray-coating is a method to deposit films out of solution by applying pressurized gas. Three steps of the process can be distinguished: atomization of the liquid by gas flow, transport of the droplets to the substrate and deposition itself [1]. In the first step, pressurized gas flows through tight nozzle, what leads to increase of its velocity. Consequently solution is sucked from the reservoir and atomized. Due to expansion of liquid flux after the nozzle, a cone is formed. The droplet density in the cone decreases with the distance from the nozzle. The cone can be divided into three regimes: dense

(DE), diluted (DI) and very diluted (VD) - see figure 1. Sample-to-nozzle distance is a crucial parameter for spray deposition, one should choose it in order to be located somewhere in between DI and VD regimes. That is because in that region isolated, small droplets occur.

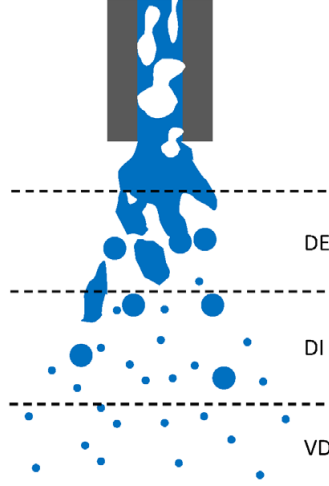


Figure 1: Schematic representation of three flow regimes [2]

Last step of the spray deposition process is determined by solid-liquid interactions. The wetting behaviour of the substrate has a huge impact on final shape of deposited film and must be taken into consideration. After the droplets land on the surface, the solvent evaporation process starts and the fluid kinetics start to dominate. Therefore, temperature of the substrate and concentration of material in the solution as well as solvent's type are crucial parameters in spray deposition.

Spray coating is a widely used method as it allows to obtain large and homogeneous layers. From application point of view another important feature is, that relatively low amount of material is wasted during the coating process. Spray deposition is applied in photovoltaic, energy storage devices, production of transparent, semiconductor or conductive coatings, power electronic applications, organic electronics and catalysis [1].

2.2 Grazing incidence small angle x-ray scattering

Electromagnetic radiation in x-ray energy range relatively weakly interacts with matter. The refractive index of x-rays is slightly smaller than unity. It can be expressed by formula

$$n = 1 - \delta - i\beta,$$

where $\delta, \beta > 0$ and δ is related to dispersion, whereas β is an absorption term. As one can easily proof using Snell's law, the consequence of n smaller then 1 is the total external reflection occurring for angles of incident beam smaller then so called critical angle ($\alpha_c \simeq \sqrt{2\delta} \simeq 0,1^\circ \div 0,5^\circ$). When incident angle is smaller than α_c beam is totally

reflected with only evanescent wave present inside the material. For incident angles α_i close to critical angle, penetration depth is strongly reduced by reflection effects [3]. This effects allow to probe thin layers as the signal from underlying substrate is reduced.

In GISAXS the angle between direction of incident beam and sample's surface is low ($\alpha_i < 1^\circ$). The geometry is shown on the figure 2. The momentum transfer \vec{q} is defined as $\vec{q} := \vec{k}_i - \vec{k}_f$, where \vec{k}_i is a wave vector of incoming beam, and \vec{k}_f - wave vector of scattered beam.

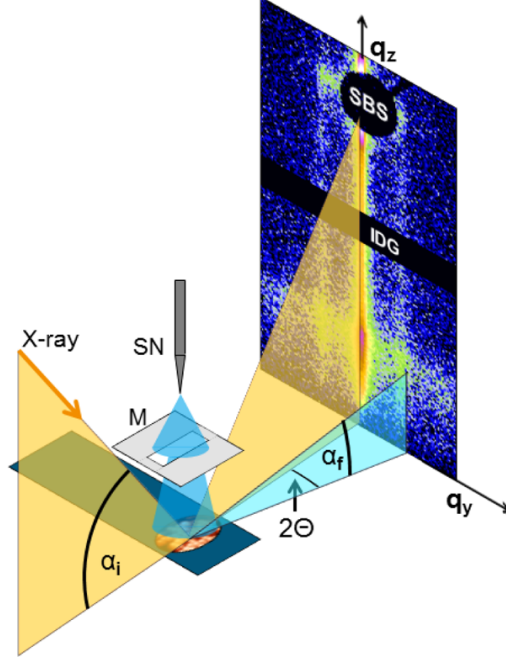


Figure 2: Geometry of GISAXS experiment [4]

Angles α_i of incident beam and α_f of scattered beam are given with respect to the sample's surface. 2θ is an angle with respect to the plane spanned by \vec{k}_i and q_z axis. These angles can be easily connected to components of \vec{q} by the following formulas, under assumption that scattering is elastic

$$q_x = \frac{2\pi}{\lambda} [\cos(2\theta) \cos(\alpha_f) - \cos(\alpha_i)],$$

$$q_y = \frac{2\pi}{\lambda} [\sin(2\theta) \cos(\alpha_f)],$$

$$q_z = \frac{2\pi}{\lambda} [\sin(\alpha_f) + \sin(\alpha_i)].$$

In GISAXS values of $q_x \ll q_y, q_z$, so q_x can be neglected [1]. Range of probed q values depends on sample-to-detector distance. Resolution is connected with pixel size of the detector as well as incident beam's divergence.

In fig. 3 a typical GISAXS 2D pattern obtained directly from the detector is shown together with characteristic features indicated.

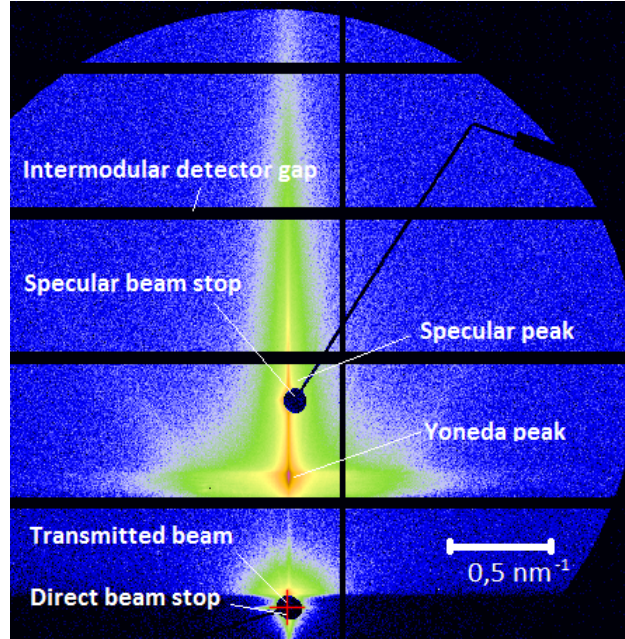


Figure 3: Example GISAXS 2D pattern with characteristic features indicated

Incident beam is scattered both specularly and diffusely. Specular peak occurs for $\alpha_f = \alpha_i$ and is a result of the specular reflection of incoming beam. Yoneda peak appears for $\alpha_f = \alpha_c$ and is a result of interface phenomenon between the incident and transmitted x-ray beam [1]. Transmitted beam position defines the origin of reciprocal space and occurs at $\alpha_f = -\alpha_i$.

In order to analyse the GISAXS image, horizontal (along q_y axis) and vertical (along q_z axis) cuts are made. Obtained relations $I(q_y)$ and $I(q_z)$ give an information about distances parallel to sample's surface and about parameters like height, thickness, roughness, respectively.

From theoretical point of view, scattering in GISAXS regime is described by so called Distorted Wave Born Approximation (DWBA). For small q values kinematic theory of diffraction fails, as dynamical effects like reflection and refraction play more important role. Measured intensity is proportional to the product of form factor f and structure factor F [1]

$$I(q) \propto |f(q)|^2 |F(q)|^2.$$

Function $f(q)$ is a modified form factor known from transmission SAXS (small angle x-ray scattering) - amplitude scattered by entire object. Modified form factor is a coherent sum of several terms taking into account different possible combinations of reflection and scattering [1]. Structure factor is related to the arrangement of objects like nanoparticles on the surface.

3 Experimental section

3.1 Sample preparation

As it was already mentioned, there are several important parameters of spray-coating, that have an impact on final sample's properties. Many of these parameters are correlated to each other, what makes optimizing the deposition process more difficult.

Spray rate has a direct influence on the amount of deposited material. It is defined by the pressure of gas and the size of the nozzle. The amount of deposited material is also strictly related to the time of spraying. Nozzle-to-sample distance (NSD) influences the quantity of sprayed material as well, as bigger distance increases the area covered by the spraying cone. Both temperature and time structure of the process (number and duration of breaks) can also have an impact on final sample's properties.

In fig. 4 the sample preparation set-up is presented.

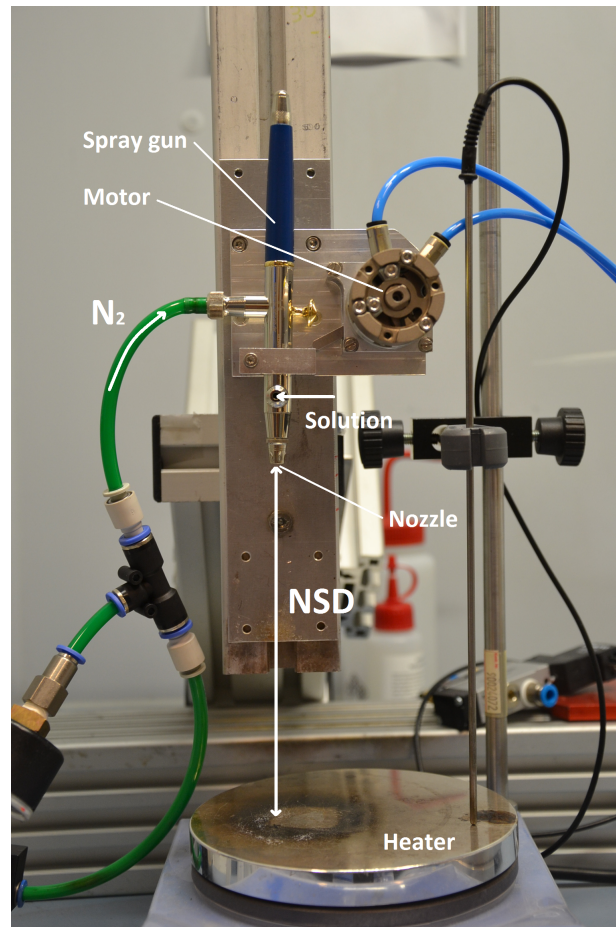


Figure 4: Spray deposition set-up for sample preparation

Sample is placed on the heater in order to control substrate's temperature. Opening and closing of gas flow is operated automatically by the motor connected to the computer.

Nanowires were already suspended in isopropanol (concentration 0,5%). Then the solution was diluted in proportion 1:7. Before deposition, the solution was put into ultrasound bath for 5 min in order to achieve better separation of nanowires. Two different kinds of silver nanowires produced by Sigma-Aldrich co. were used - large with size indicated by producer: $115 \text{ nm} \times 20 \div 50 \text{ }\mu\text{m}$ and small: $60 \text{ nm} \times 10 \text{ }\mu\text{m}$. Most samples were prepared with the use of large ones as it is presumably easier to achieve conductivity of the samples in that way.

Square glass substrates with size $\sim 2,5 \times 2,5 \text{ cm}$ were used for preparing samples. Substrates were cleaned by piranha solution ($\text{H}_2\text{SO}_4 + \text{H}_2\text{O}_2$) in order to improve their hydrophilic properties. Afterwards they were cleaned by distilled water and dried by nitrogen flow.

Spray rate was determined by the following simple method. Distilled water was sprayed for 10 s into the reservoir, which mass was measured before and then after the spraying. The procedure was repeated five times to estimate average spray rate. In order to calculate mass of the solution deposited on the substrate, the spray rate per area needed to be determined. That was done by spraying a given amount of solution on a paper and measuring the diameter of obtained wet circle. This allowed to estimate the opening angle of spraying cone, which was found to be slightly different for different sample-to-nozzle distances. This fact may be connected with evaporation of solvent, as obtained opening angle values decrease with increasing NSD.

In total 44 samples were prepared under different conditions. Among these there are a few series of samples, for which one parameter is varied, whereas the others are kept constant. That allowed to establish several relations between parameters of deposition and sample's resistance, transmission and surface coverage. Comparison of different dependencies allowed to establish a set of optimal parameters. Concentration of nanowires was not changed during preparation of series of samples. Also spray rate was kept approximately constant for most of the samples, excluding the ones prepared with different gas pressure.

3.2 Initial characterization

3.2.1 Conductivity measurements

Resistance of the samples was determined with the use of very simple method. Two electrodes made of silver paste were put on sample's surface at the distance $\sim 1,5 \text{ cm}$. Resistance was measured by multimeter as showed on the figure 5. Obtained results are in the range $[24, 4 : \infty] \Omega$.

3.2.2 Optical microscopy

Optical microscopy was done in order to check samples morphology using the most simply available method. Microscope Keyence VH-Z250R, which allows to achieve magnifications up to 2500 times, was used. Two micrographs for one of conductive samples are presented on the next page (fig. 6). As one can see, arrangement of nanowires on

the surface is chaotic and no alignment can be distinguished. From the picture with lower magnification it can be seen that layer is quite homogeneous.



Figure 5: Conductivity measurements with the use of digital multimeter

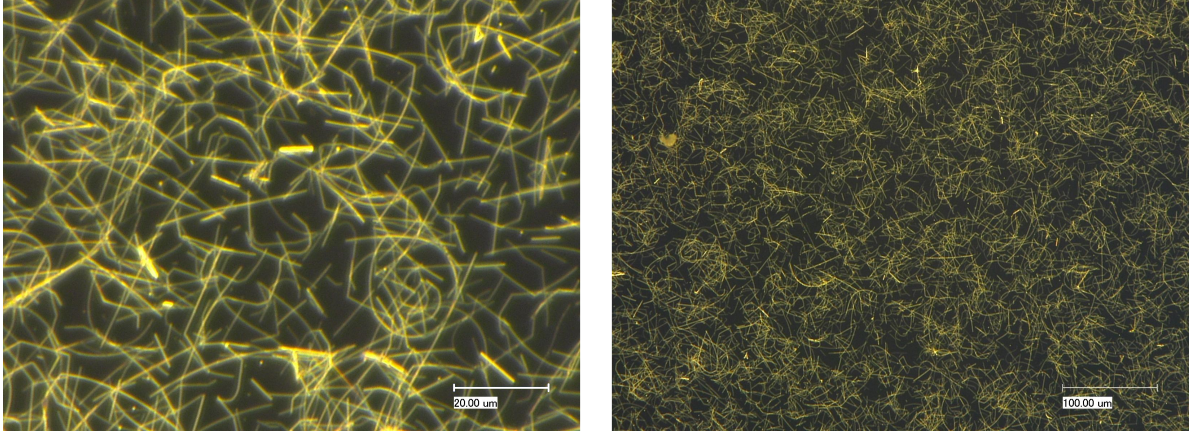


Figure 6: Optical micrographs with magnification $2500\times$ (left) and $500\times$ (right)

Based on obtained micrographs, determination of samples coverage was done using ImageJ programme. Contrast and threshold were adjusted and area not covered with nanowires measured. The procedure was performed for three micrographs with magnification $2500\times$ for each sample in order to obtain average value. Pictures were taken for points between two electrodes, where the concentration is the highest.

It is important to mention, that method described above is not accurate. It could be seen from values obtained for given sample, which varied quite significantly. Mean standard deviation for all samples was equal to $\sim 0,051$.

For one sample, prepared under the following circumstances: gas pressure $p = 1$ bar, $NSD = 11$ cm, absolute spray rate $v_s = 0,088$ g/s, effective spray rate $v_s^* = 0,01$ g/(s·cm²), time of spraying $t = 8$ s, substrate's temperature $T = 80^\circ\text{C}$, mass of deposited

solution $m = 0,5$ g, time structure of the process: 2 s of spraying, 1 s of break and so on, 25 pictures were taken at different positions on sample's surface in order to determine how the concentration changes with position. Resistance of this sample was found to be $R = 41,2 \Omega$. Obtained relation between concentration of nanowires and position is presented below together with a few pictures corresponding to different positions. Area not covered by nanowires is marked by red colour.

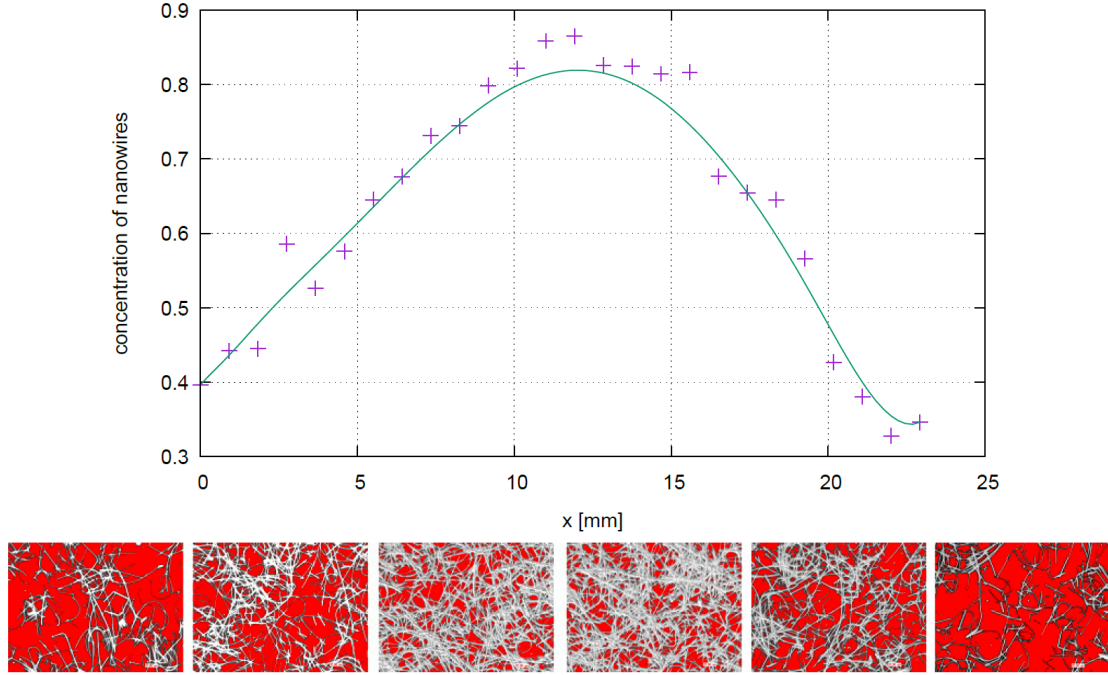


Figure 7: Plot of surface coverage against position on sample's surface together with example micrographs

As one can see on the plot (figure 7), there exists a range on samples surface with a length of about 8 mm, where the concentration of nanowires is the highest and approximately constant. Apart from that range, it gradually decreases when going to the edges.

The comparison of values obtained from concentration determination and resistances lead to the conclusion, that coverage needs to be higher than approximately 0,55 in order to achieve conductivity of the layer. Resistance values lower than 100Ω are characteristic for samples with surface coverage higher than 0,7.

3.2.3 Transmission measurements

Transmission coefficient determination for selected samples were performed by BWTEK Inc. Glacier X UV-Vis spectrometer. The measurement's principle is very simple - intensities of incoming and transmitted beam are determined and transmission calculated as the ratio of those two. In practice procedure is the following: a measurement of spectrum

for covered light source (dark scan, without beam) is recorded to get information about background. Then scan without sample is done to measure the incident beam's intensity (bright scan), taking into account previously measured background. Values obtained for each wavelength are then treated as 100% transmission for further measurements.

Transparency was checked for a series of 4 samples prepared under different conditions, what led to different resistance values and coverages of surface. The parameters of samples are collected in the table below. Parameters common for all samples: $p=1$ bar, $NSD=11$ cm, $v_s=0,087$ g/s, $v_s^*=0,01$ g/(s·cm²), $T=80^\circ\text{C}$.

Table 1: Parameters of samples for which transmission was determined

No.	t [s]	m [g]	time structure	R	coverage
1	3	0,184	no breaks	12 M Ω	0,43
2	8	0,490	4s, break: 2s, ...	75 k Ω	0,61
3	10	0,613	no breaks	234 Ω	0,78
4	12	0,736	no breaks	52,2 Ω	0,82

The obtained spectra are shown on the graph below (fig. 8). Additionally the empty substrate was measured.

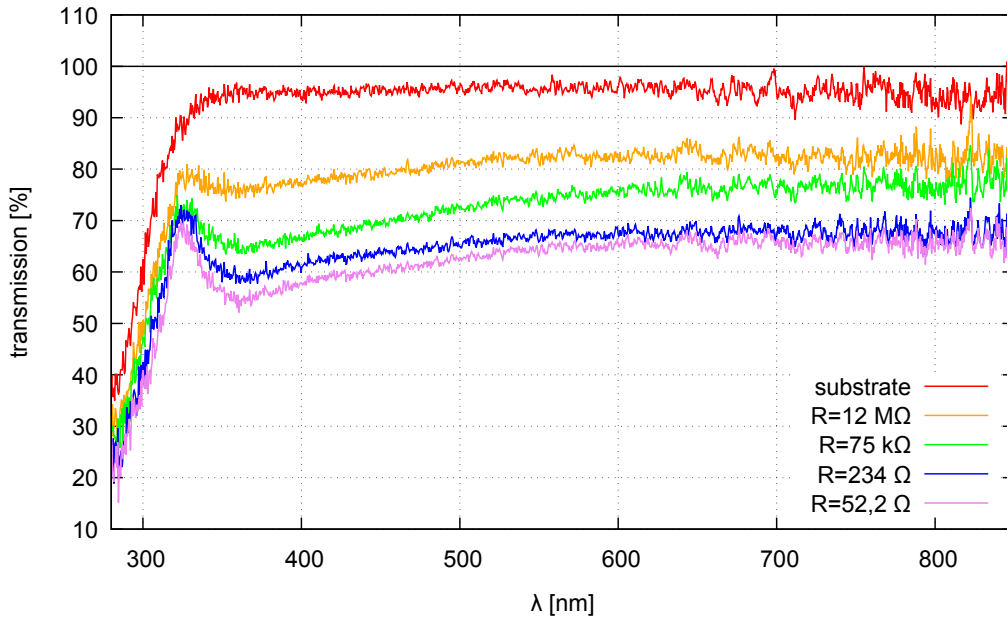


Figure 8: UV-Vis spectra of Ag nanowire thin films

Already from presented spectra one can see, that there is a correlation between the resistance or surface coverage and transmission. For the most conductive sample the transparency is also highly reduced.

In order to obtain a single parameter for each sample characterizing its transparency, an average value of transmission coefficient was calculated for visible range ([390;800] nm). Relative transmission coefficient defined by the formula

$$T_{rel} = \frac{T}{T_{substrate}},$$

was used as the desired parameter. Below a graph with obtained values in dependence of resistance is shown.

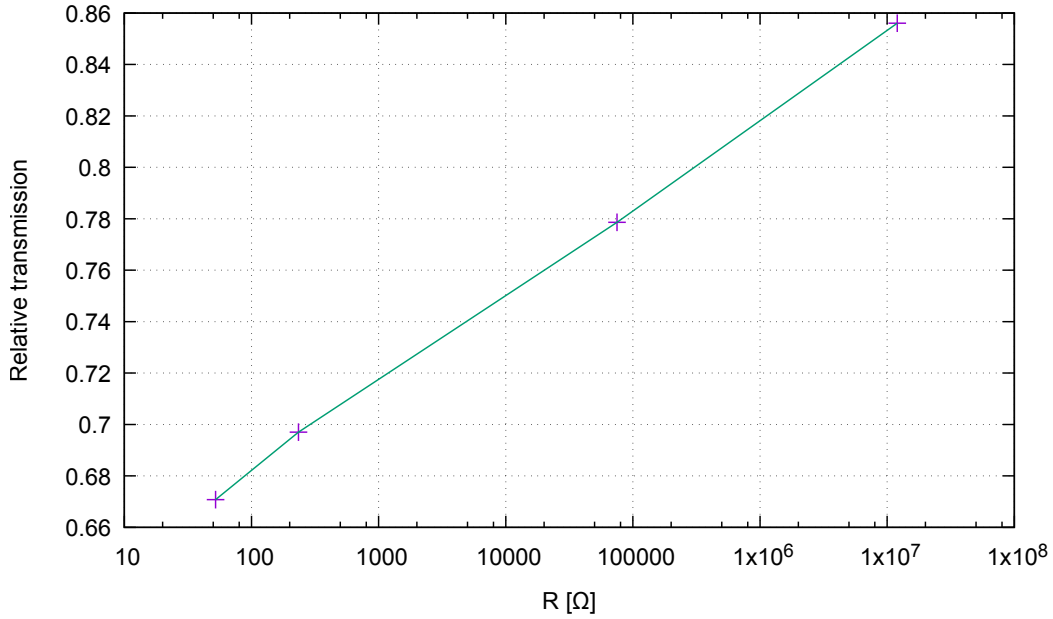


Figure 9: Plot of relative transmission coefficients T_{rel} against resistance of the sample

The plot is with a good approximation a linear function but it is important to emphasize, that the x axis is with a logarithmic scale. It means that transmission linearly depends on the order of magnitude of resistance. On the next plot (fig. 10) a dependency of average relative transmission on surface coverage is presented. The data points nearly perfectly form a linear function - transmission linearly decrease with increasing concentration. This is an important result from application point of view. One need to take it into consideration, when looking for not only optimal resistance, but also good transparency.

3.3 Relations between properties and deposition parameters

Determination of resistance and surface coverage for all samples, as well as transmission coefficient (already discussed, section 3.2.3) for selected samples, enabled to establish a few dependencies of those values on deposition parameters. Most of these are dependencies on resistance, as determination of conductivity was presumably more accurate.

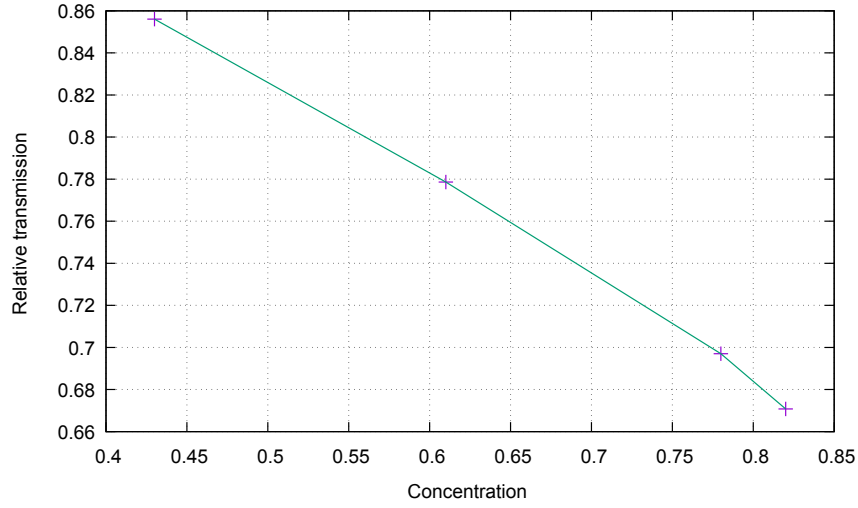


Figure 10: Plot of relative transmission coefficients against concentration of nanowires

3.3.1 Temperature of the substrate

A series of 6 samples was prepared with varied substrate temperature. Common parameters: $p=1$ bar, $NSD = 11$ cm, $v_s=0,091$ g/s, $v_s^* = 0,01$ g/(s·cm²), $t = 5$ s, $m=0,32$ g. Temperature was changed from 20°C (room temperature) to 50 °C and then to 170°C with a step of 20°C.

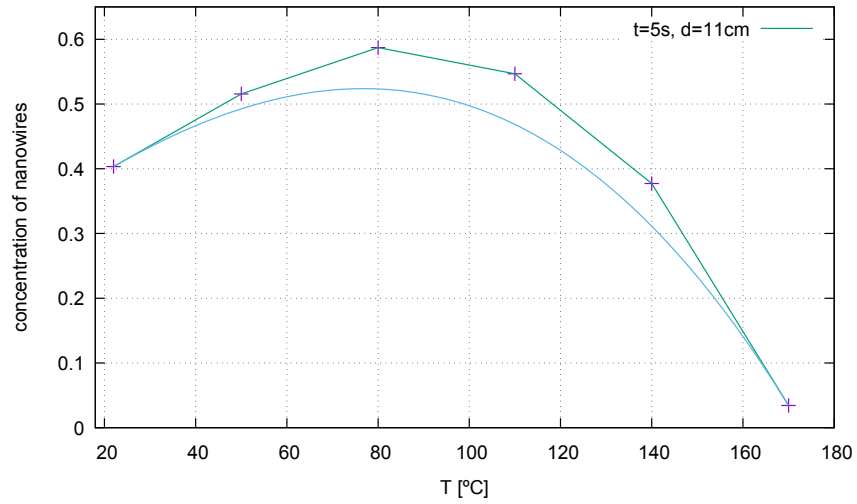


Figure 11: Dependency of concentration of nanowires on substrate's temperature

Highest concentration was obtained for temperature of substrate around 80°C. For both higher and lower temperatures concentration decreased. For high temperatures it might

be related to evaporation of solvent during the flight to the surface. In case of small temperatures a wet film is formed on the substrate's surface, what can lead to the agglomeration of nanowires. In this case concentration was chosen as a variable, since most of the samples were not conductive.

3.3.2 Time of spraying

Dependency of resistance on time of spraying was determined for three series of samples (different NSD - 11, 13, 15 cm). All of these showed very similar behaviour, so only one will be presented in details. Common parameters of deposition: $p=1$ bar, $NSD=11$ cm, $v_s \simeq 0,085$ g/s, $v_s^* = 0,01$ g/(s·cm²), $T = 80^\circ\text{C}$, no breaks.

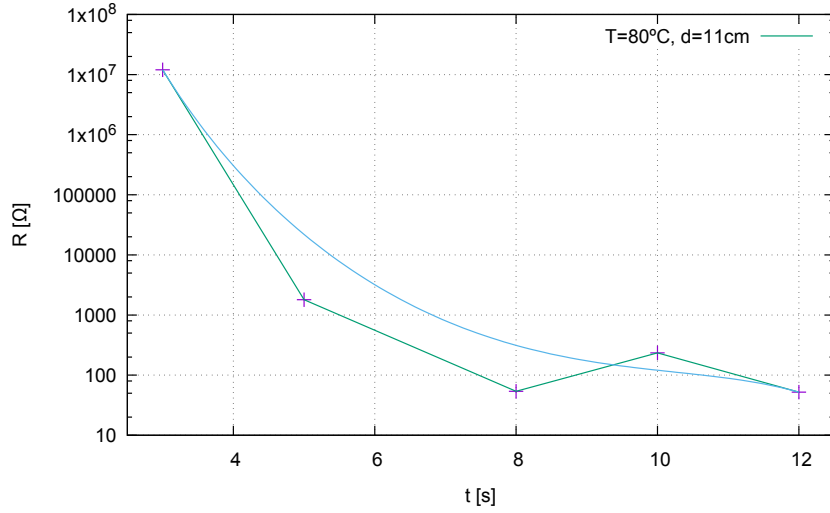


Figure 12: Dependency of sample's resistance on time of spraying

As it can be seen, resistance decreases with increasing time of spraying. This result was expected, as time of spraying is directly related to the amount of deposited material. It is also worth to mention, that after some point further increase of time do not change the value of resistance dramatically (it is the same to the order of magnitude).

3.3.3 Time structure of the process

In the next step, the issue how samples' properties depend on the number and duration of breaks and the duration of spraying in between was investigated. As an example a series of three samples with the following common parameters: $p=1$ bar, $NSD=13$ cm, $v_s \simeq 0,085$ g/s, $v_s^* = 0,008$ g/(s·cm²), $t = 12$ s, $T = 80^\circ\text{C}$, is presented.

As one can conclude by comparison of values collected in table 2, introduction of short breaks between spraying seem to improve sample's parameters (conductivity, surface coverage). What is more, based on these results, it seems that breaks should not be too long, they need to be shorter than the time of spraying. The other prepared series

of samples with smaller NSD (11 cm) gave very similar result, with one exception, what could be caused by some random changes in deposition conditions.

Table 2: Cycle-type dependence of samples' resistance

No.	cycle	m [g]	R	coverage
1	no breaks	0,62	188,4 Ω	0,57
2	2, (1), ...	0,56	24,4 Ω	0,69
3	2, (2), ...	0,56	39,6 Ω	0,67

3.3.4 Nozzle-to-sample distance

Finally, the dependency of resistance on NSD was determined. Two series of samples were prepared, with various time of spraying (8 s and 12 s). Both showed the same trend. Common parameters: $p=1$ bar, $v_s \simeq 0,085$ g/s, $T = 80^\circ\text{C}$, $t = 8$ s, no breaks.

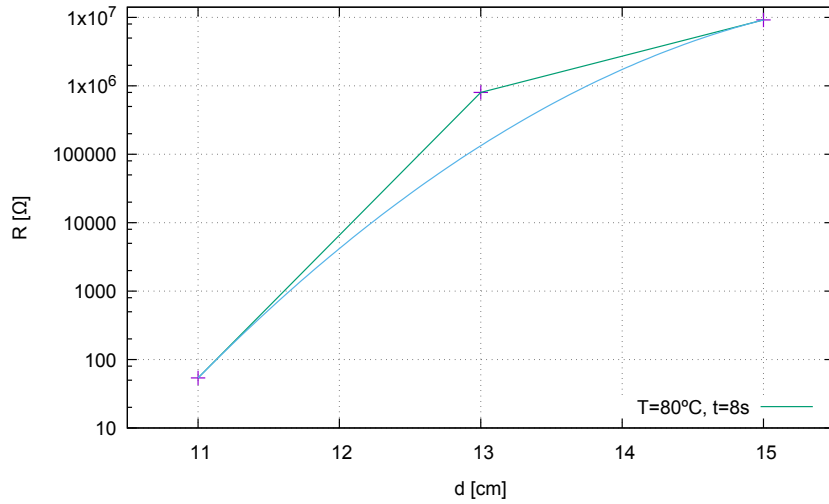


Figure 13: Dependency of sample's resistance on NSD

Resistance increases with increasing NSD, what is related to the change in effective spray rate (spray rate per area). One would need to increase the time of spraying in order to compensate this effect. But it is not advised, hence it will also lead to increase in waste generation.

3.3.5 Size of nanowires

Up to this moment, all presented results were obtained for samples prepared out of large nanowires. 8 samples were prepared with the use of small nanowires, under different conditions. Similar dependencies were obtained as for large ones. The main difference is that one need to spray a bigger amount of material in order to obtain conductivity, what

can be seen on the next graph (common parameters: $p=1$ bar, $NSD=11$ cm, $v_s=0,075$ g/s, $v_s^*=0,008$ g/(s·cm²), $T = 80^\circ\text{C}$, no breaks).

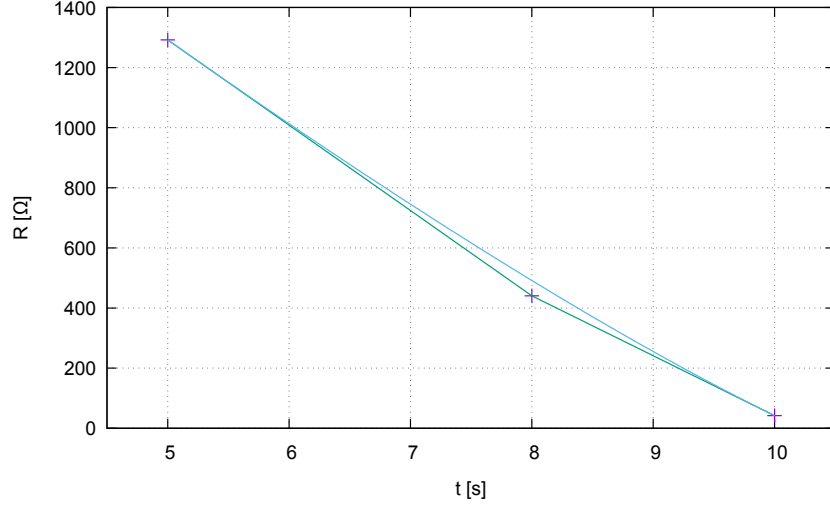


Figure 14: Dependency of sample's resistance on time of spraying for small nanowires

For large nanowires resistance below 100 Ω was reached already for 8 s (fig. 12). As it can be seen on the graph, in case of small nanowires a region where resistance is approximately constant is not reached up to 10 s.

3.3.6 Final remarks, set of optimal parameters

Taking into account all obtained results, the following set of parameters as optimal for nanowire thin film preparation was established for given spray rate $v_s \simeq 0,08$ g/s, $v_s^* = 0,01$ g/(s·cm²) and pressure $p = 1$ bar.

Table 3: Set of optimal parameters

t [s]	NSD [cm]	T [°C]
8	11	80

NSD was chosen small in order to avoid unnecessary waste generation.

3.4 Atomic force microscopy

The fact, that nanowires with thickness about 100 nm could be so well resolved by optical microscope was already quite unexpected. Their diameter is meant to be way below the shortest wavelength of visible light, so in principle it should be impossible. For this reasons, AFM measurements were conducted, as this method allows to achieve higher magnifications.

In AFM, image is obtained after the computer analysis of the signal obtained from tap located over the surface of investigated material. The force exerted by the material on the tap depends on the distance (Hook's law). The force is kept constant, so the height differences can be recorded.

Measurements were performed with the use of NT-MDT NTEGRA Aura System AFM microscope. Surface of one sample was investigated (samples parameters: $p=1$ bar, $NSD=11$ cm, $v_s=0,09$ g/s, $v_s^*=0,01$ g/(s·cm²), $m=0,32$ g, $T=20^\circ\text{C}$, no breaks, $R \rightarrow \infty$, coverage=0,4). Non conductive sample with relatively low surface coverage was chosen, since samples with low roughness are better for AFM measurements. In the fig. 15, an example AFM micrograph is presented together with a profile of one nanowire (marked on the micrograph).

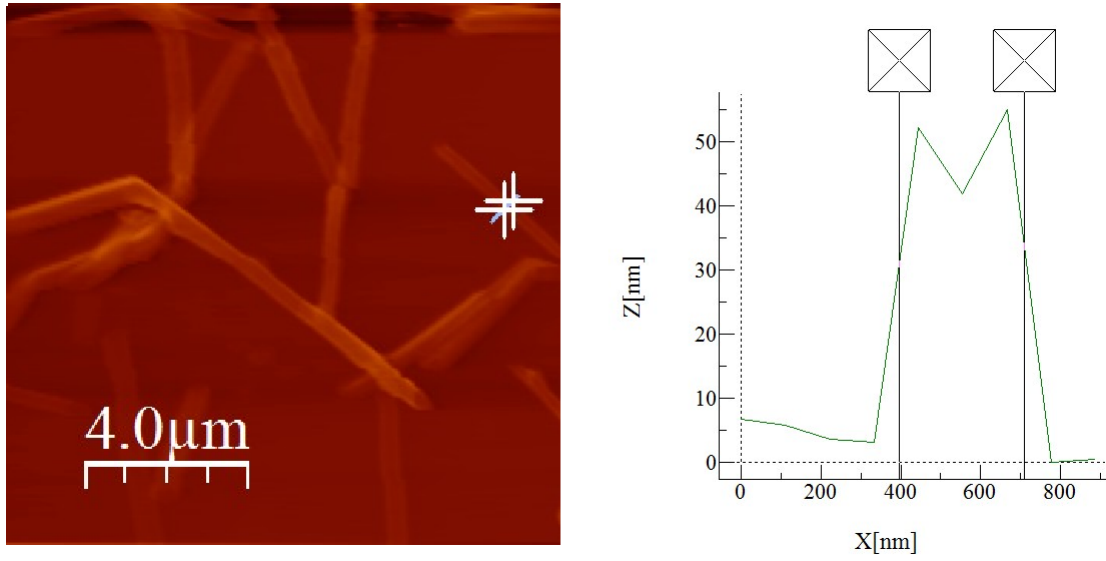


Figure 15: AFM micrograph and profile of nanowire obtained from the image

Thickness of 20 nanowires was measured on different AFM micrographs via the programme WSxM 4.0 Beta 9.0 [5]. The following average value was obtained: $388,3 \pm 70,3$ nm. The same procedure was repeated with optical micrographs with ImageJ programme and the following thickness obtained: $589,5 \pm 129,7$ nm. Both values are the same to the order of magnitude. Both are a few times bigger than thickness declared by the producer.

The shape of profile of nanowires obtained from AFM is absolutely not consistent with what one would expect. Height on the graph is 10 times smaller than obtained lateral thickness. That might indicate, that obtained results are not reliable. Such behaviour might be caused by relatively high surface coverage - the tap "feels" the nanowires all the time and do not probe lateral distance differences correctly.

Just at the end of the Summer Student Programme, small angle x-ray scattering experiment was conducted for nanowires suspended in isopropanol. Solutions with different concentration of nanowires were investigated. The brief analysis confirmed, that

thickness of nanowires is very similar to the values indicated by the producer. Different size seen on optical micrographs can be caused by diffraction effects, as thickness of nanowires is comparable to the wavelength.

3.5 GISAXS measurements

3.5.1 General description

Measurements were performed at PETRA III (ger. Positron-Elektron Tandem Ring Anlage) synchrotron radiation source. Electromagnetic radiation in wide energy range is produced in storage rings by bending magnets or insertion devices (undulators and wigglers). For all these devices the principle behind is acceleration of charged particles - as known from classical electrodynamics, such particles radiate electromagnetic wave. Produced radiation is linearly polarized in the plane of the ring.

Beamline P03 located in PETRA III provides conditions suitable to perform GISAXS experiments. Apart from this, GIWAXS, SAXS and WAXS can be also conducted. Radiation is produced by undulator. Beamline consists of three hutches: optics hutch, experimental hutch 1 (micro-focused) and experimental hutch 2 (nano-focused) [6]. In this experiment 2D detector Pilatus 1M with pixel size $0,172 \times 0,172 \text{ mm}^2$ was used.

GISAXS experiments were performed for a series of three samples prepared out of large nanowires and for one sample with small nanowires on the surface. For each of them a scan was performed over the range of positions between two silver electrodes (region of interest). The step was chosen to be 0,1 mm and distance around 8 mm, so approximately 80 images were recorded for each sample. Incident angle was chosen equal to $0,45^\circ$.

3.5.2 Alignment

Before performing a scan, a sample need to be appropriately aligned on the sample holder. Positioning is done remotely by engines connected to the computer in control hutch. A beam shutter is opened and position of the beam with respect to the sample's surface checked by measuring intensity on the diode, which is placed on the direct beam stop. Firstly, vertical coordinate is changed in order to place sample so that beam hits sample's edge. Position is fixed in the point where intensity on the diode is at the half of its maximum. Next, the tilt of the sample is changed in order to find the position where surface is parallel at this point to the beam. It is now defined by the angle's value, where the beam's intensity on the diode is the highest. This procedure is repeated several times to get to desired position as close as possible. Finally, the horizontal position of the sample is changed, as sample might be still tilted in the plane spanned by z axis and direction perpendicular to the beam, and entire process described above repeated.

3.5.3 Calibration

Sample-to-detector distance (SDD) and wavelength are determined empirically. In order to obtain the first parameter, a scan over the range of incident angle values was

performed. In total 61 images were recorded and incident angle changed in range $[0,2^\circ : 0,8^\circ]$ with step $0,01^\circ$ (values from controlling computer). The position of specular peak was measured for each image and linear function $y = ax + b$ fitted to obtained data, as showed on the graph below (fig. 16).

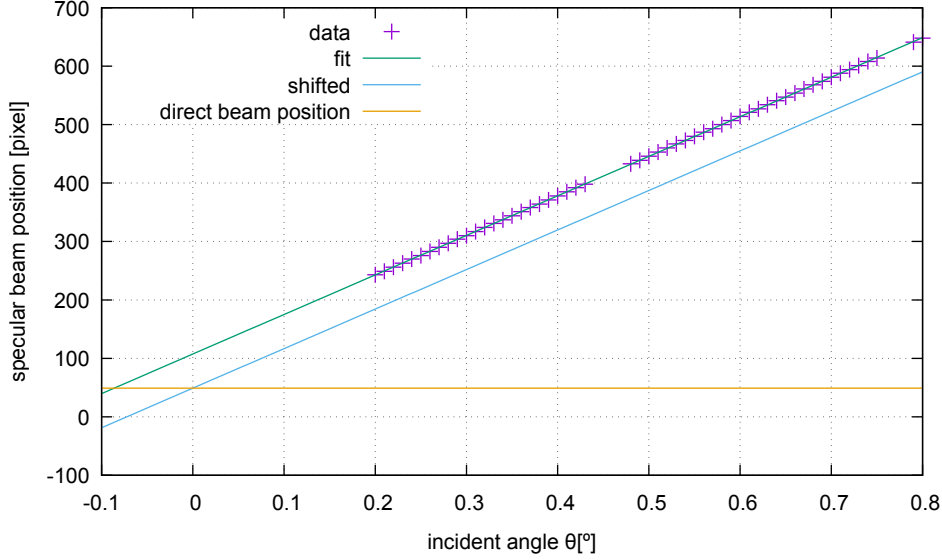


Figure 16: Specular peak positions for calibration sample

Obtained linear function was shifted in a way to get the cross point of the function and value of direct beam position for incident angle $\theta = 0$. It is done to properly define the scale of angles - incident angle should be 0 for direct beam. The function need to be shifted along x axis by the value $\tilde{x} = |(y_0 - b)/a|$, where y_0 is the position of direct beam. Such an obtained function is a calibration plot for a given experiment. For each position of specular beam now a real value of α_i can be calculated by using the equation of shifted line:

$$y = 676,64 \alpha_i + 49 \quad \Rightarrow \quad \alpha_i = \frac{y - 49}{676,64}.$$

Value of the slope of the line a is nothing but the number of pixels per unit, 1° in this case. As the pixel's size is known, from this data one can easily calculate SDD based on triangle with $\xi = 1^\circ$ and $A = a \cdot \text{pixel size}$, $B = \text{SDD}$. Therefore

$$\text{SDD} = \frac{a \cdot \text{pixel size}}{2 \tan(1^\circ)}.$$

Factor 2 comes from the fact that incident angle is half of ξ . Value obtained in this case: $\text{SDD} = 3334 \text{mm}$.

Wavelength is obtained from transmission SAXS measurements of the material which structure is well known (interplanar spacing) - Ag Behenate ($d_{001} = 58,38 \text{ \AA}$) in this case. Peak positions are obtained by fitting in DPAK v1.2.0 programme [7] and via Bragg's law wavelength is obtained. In this case its value was equal to $0,9484 \text{ \AA}$.

3.5.4 Results

Below (tab. 4) the parameters of measured samples are collected. Common parameters: $p=1$ bar, $t = 8$ s, $v_s \simeq 0,08$ g/s, $T = 80^\circ\text{C}$, no breaks.

Table 4: Parameters of samples measured by GISAXS

No.	NSD [s]	m [g]	v_s^* [g/(s·cm ²)]	R	coverage
1	11	0,46	0,009	53,8 Ω	0,69
2	13	0,41	0,008	0,8 M Ω	0,48
3	15	0,32	0,006	9,2 M Ω	0,31
4	11	0,42	0,008	440,5 Ω	0,82

As it was already mentioned, samples 1-3 were prepared from large nanowires, in opposite to sample 4, which is made of small ones. Samples 1-3 show different resistance values, what is obviously connected with their surface coverage. Both of these two parameters were influenced by different NSD in this case.

Comparison of example GISAXS patterns for all samples is shown below.

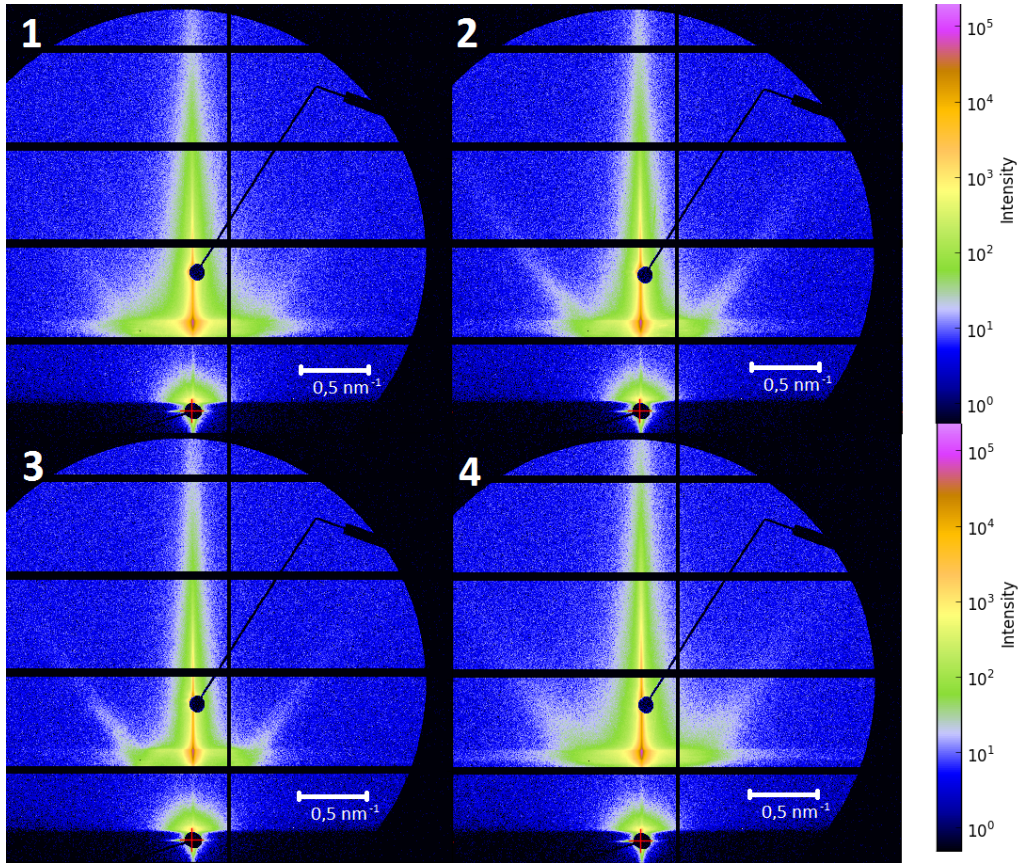


Figure 17: Example GISAXS patterns for samples 1-4

As it can be clearly seen, significance of the patterns' features changes from sample to sample, so one may conclude that it depends on the concentration of nanowires. As concentration decreases from 1 to 3, less intense pattern is observed. This fact causes the increase of visibility of side maxima and streaks, as they are less affected by central peak intensity. All the features are already smeared out for the last image, which corresponds to the sample with the highest surface coverage. More features of the images can be seen on the comparison of vertical and horizontal cuts for these samples, which will be presented in the next chapter (3.5.5). The entire analysis of GISAXS data was performed by DPDAK v1.2.0 programme.

In the figures 19 and 20 a series of four images containing the cuts: horizontal and three vertical at different positions, for one sample is presented. Horizontal cuts were done around Yoneda peak. For vertical cuts position around central peak was chosen together with two more shifted ones. It is indicated on the figure 18.

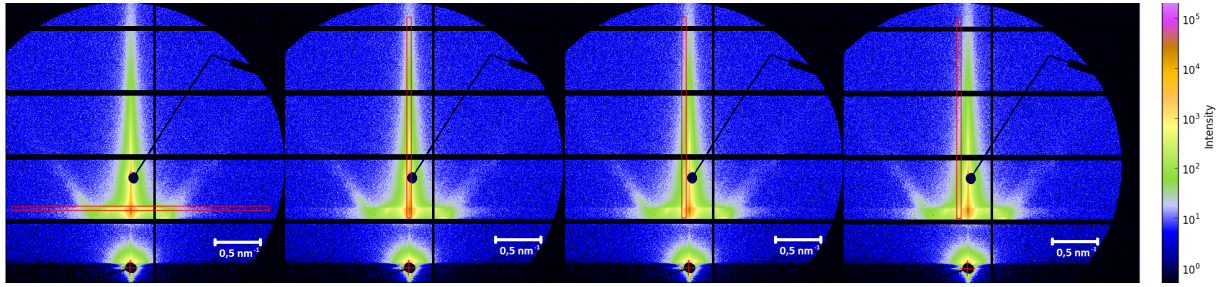


Figure 18: Positions of horizontal (1) and vertical (2-4) cuts for sample 3

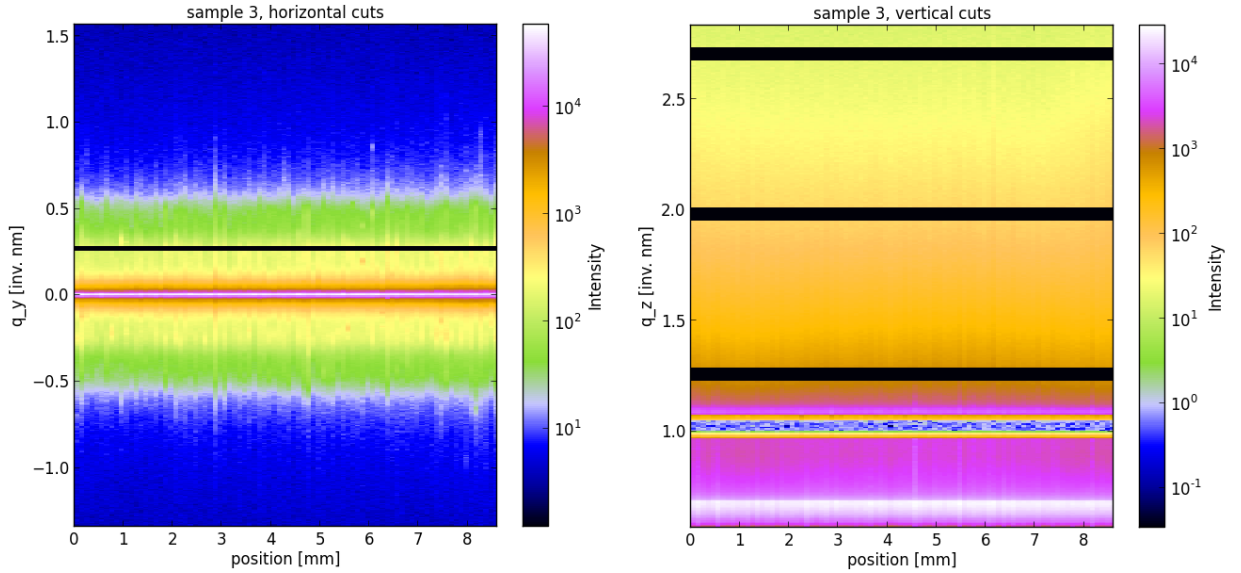


Figure 19: Horizontal (left) and vertical cuts around central peak (right) for sample 3

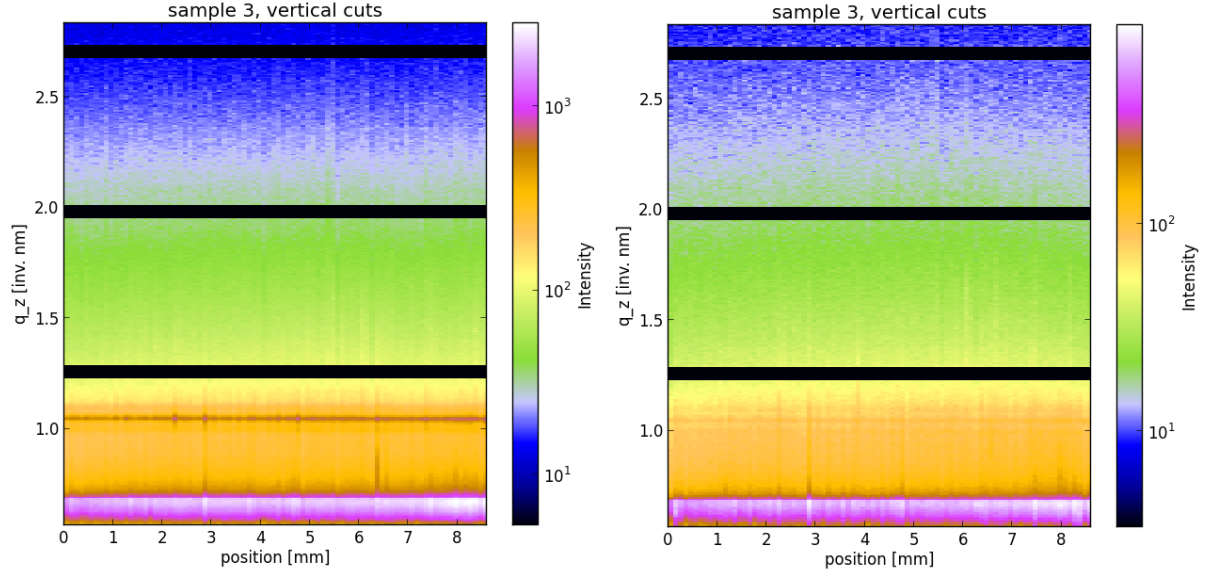


Figure 20: Vertical cuts at q_y position shifted from the origin (sample 3)

Most important conclusion that can be drawn from comparing these series of cuts is homogeneity of the coating - no drastic changes in intensity can be observed. Although some fluctuations can be seen for example in the first image, with horizontal cuts, they are not significant. This observation is supported by the shape of vertical cuts showed on figure 20. It is hard to distinguish any features on vertical cuts around central peak, as they are overlapped by high scattering at this region.

On the cuts presented on figure 20, one can notice some peaks around specular peak position ($\sim 1\text{nm}^{-1}$). The central peak, which is the most pronounced one in the left picture, is getting less intense when going to higher q_y values (shifting the region where cuts are made). This means that it is specular peak's intensity. The other two peaks remain similarly intense, so they are caused by some height modulations.

3.5.5 Analysis of GISAXS data - fitting

Due to the fact that no big differences among images taken at various positions on sample's surface could be observed, several patterns were summed (intensity was added and divided by the number of images). This procedure led to the improvement of statistics. GISAXS images after summation are presented in the figure 21.

Cuts at the same regions as previously were made for these images. On the next figure the comparison of horizontal cuts for all 4 samples is shown. Their shapes follow the previously described rule: features, side maxima on both side of Yoneda peak in this case, are most pronounced for the sample with lowest concentration. Side maxima are no longer visible for samples 1 and 4 which have the highest surface coverage. Intensity of scattered radiation increases with increasing concentration of nanowires.

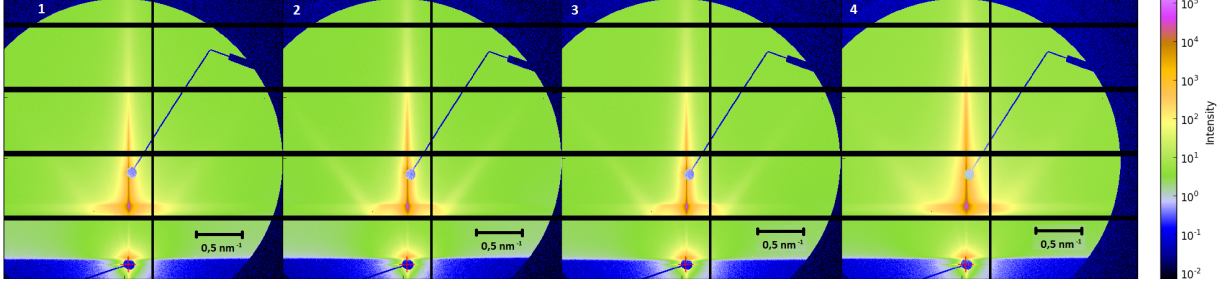


Figure 21: Collection of averaged images for samples 1-4

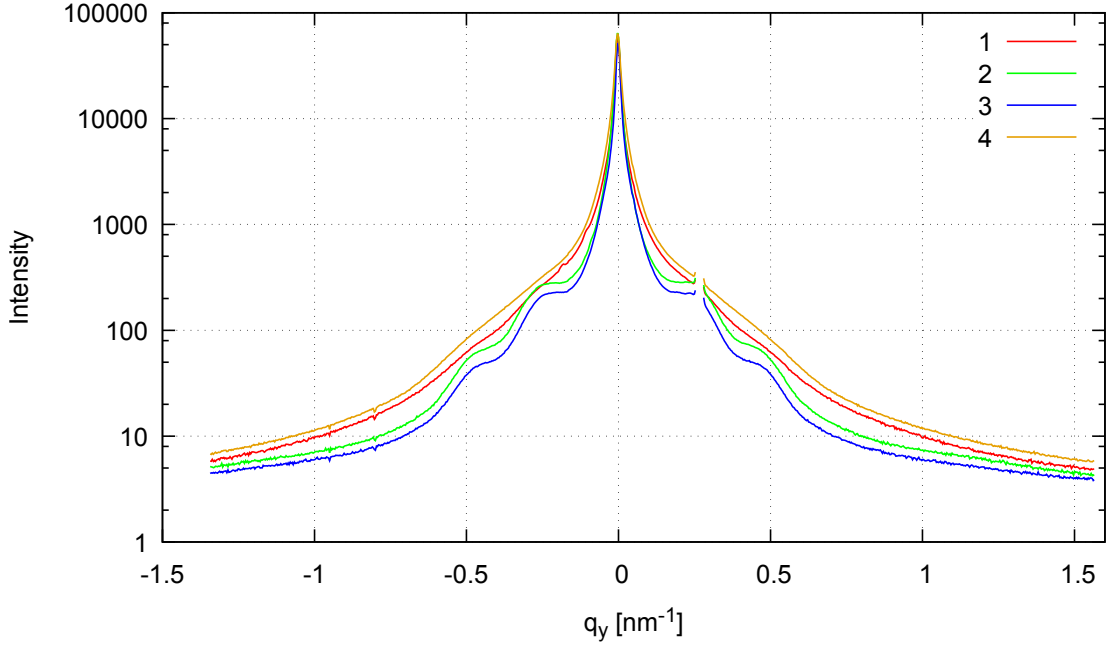


Figure 22: Horizontal cuts made on summed images for samples 1-4

The shape of horizontal cuts should be dominated by form factor of the cylinder, since there is presumably no special order of nanowires present. The analytical formula is obtained as the Fourier transform of the object shape and is the following in case of cylinder of radius R and height H [3]

$$f_{cy}(\vec{q}, R, H) = 2\pi R^2 H \frac{J_1(q_{\parallel} R)}{q_{\parallel} R} \text{sinc}\left(\frac{q_z H}{2}\right) e^{iq_z H/2},$$

where J_1 is the Bessel function of first order, $\text{sinc}(x) = \sin(x)/x$, $q_{\parallel} = \sqrt{q_x^2 + q_y^2} \approx |q_y|$ in this case. Only the term $J_1(x)/x$ is significant for the investigation of lateral distances. As one can see on the next graph, the plot of the square of this term also

shows extrema on both sides of the central maximum. Therefore, one can take the positions of $(J_1(x)/x)^2$ first two minima and then calculate the radius of cylinder with formula

$$R = \frac{x_{min}}{q_y}.$$

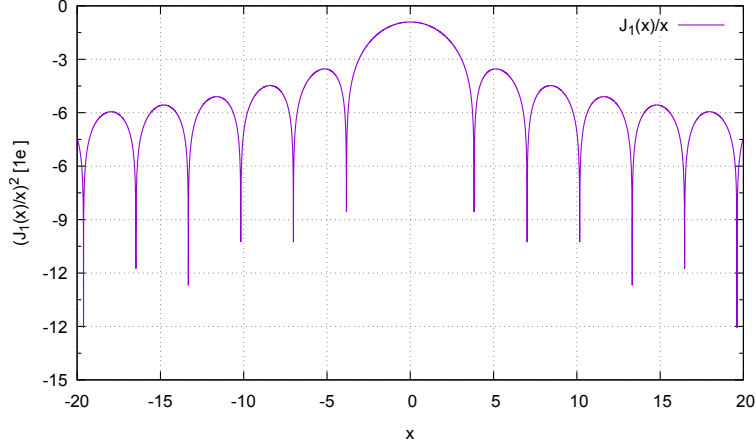


Figure 23: Plot of $(J_1(x)/x)^2$

Positions of two minima were found to be approximately 3,83 and 7,02. Values obtained for radius are collected in table below.

Table 5: Parameters of samples measured by GISAXS

No.	q_y^1 [nm ⁻¹]	q_y^2 [nm ⁻¹]	R_1 [nm]	R_2 [nm]
2	0,18	0,4	21,28	17,55
3	0,17	0,395	22,53	17,77

Obtained values seem to be too small in comparison to what is indicated by the producer of nanowires. What is more, value calculated for the second minimum is slightly smaller than the other one. This two values should be similar, as observed side maxima are of the first and second order. The difference might be caused by relatively high uncertainty of determining positions of experimental minima.

Subsequently, the vertical cuts were analysed in details. The comparison of vertical cuts made a bit apart from central peaks for all 4 samples is shown in figure 24. As one can easily see, side maxima around specular peak are again most pronounced for samples with lowest surface coverage. This time maxima for the sample 4 can be also distinguished, in case of sample 1, they are overlapped by the specular peak. For sample 3 it is even possible to observe second order peaks.

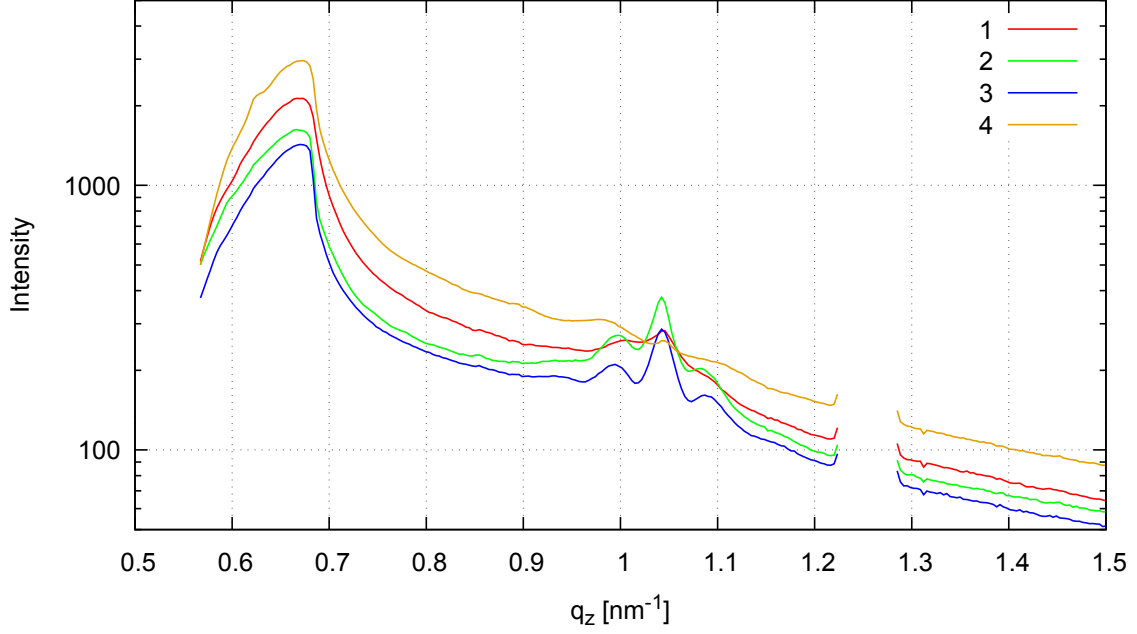


Figure 24: Vertical cuts shifted from central peak made on summed images

Functions were fitted to the cuts in order to evaluate peak positions. Lorentzian function was fitted to the specular peak position and Gaussian functions to side maxima. The functions' positions and FWHM are collected in the table below. Plots of fit results for samples 2, 3 and 4 are presented on the next page. Positions of the side maxima can be used to estimate average height modulations in the sample. This can be done by calculating the position relative to the position of central peak (specular) and consequently, computing distance d by using formula

$$d = n \frac{2\pi}{\Delta q},$$

where n is the order of the maximum.

Table 6: Parameters of samples measured by GISAXS

	Sample 2				Sample 3				Sample 4	
[nm ⁻¹]	L	G1	G2	G3	L	G1	G2	G3	L	G1
position	1,04	0,95	0,996	1,09	1,04	0,945	0,99	1,095	0,98	1,07
FWHM	0,025	0,057	0,037	0,036	0,024	0,058	0,029	0,028	0,052	0,11
Δq		0,093	0,046	0,048		0,098	0,05	0,052		0,086
d [nm]		134,5	137,0	132,1		128,6	125,5	120,7		72,8

As it can be seen in the table 6, obtained values are very close to the ones declared by the producer of nanowires. Average value for sample 3 (124,9 nm) is with better agreement with the latter (115 nm). For this sample the nanowires can be easier resolved, since the surface coverage is smaller. The highest difference ($\sim 20\%$) between obtained value and nominal one is observed for sample 4 prepared out of small nanowires.

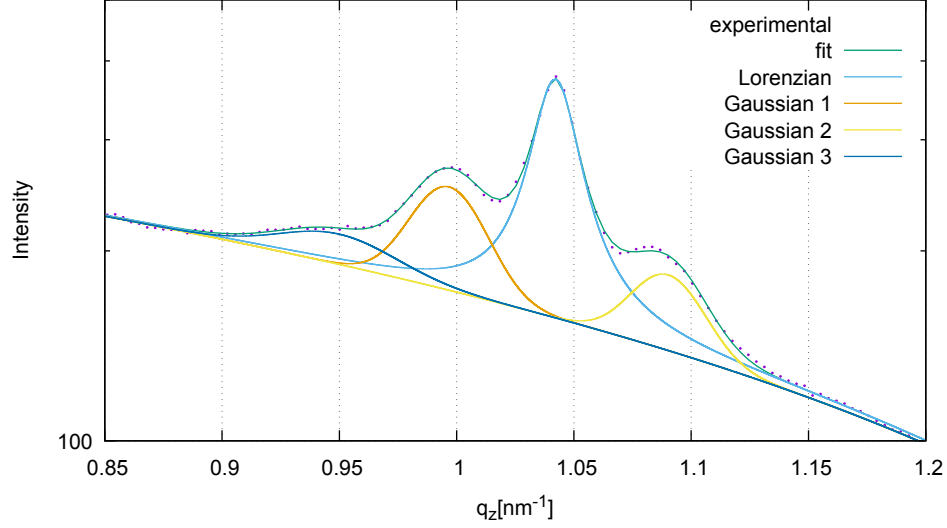


Figure 25: Vertical cut, fit results for sample 2

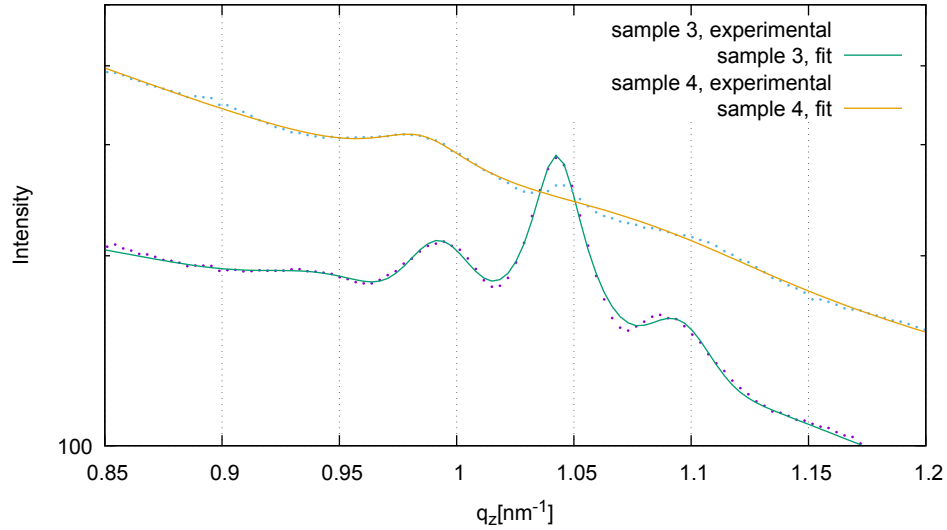


Figure 26: Vertical cut, fit results for samples 3, 4

Some side maxima can be also observed around Yoneda peak. They are located around $0,45 \text{ nm}^{-1}$ to the sides from central peak. Additional vertical cuts were made around this area for samples 2-4, as the maxima cannot be seen on the sample's 1 pattern. Comparison of obtained cuts is shown below.

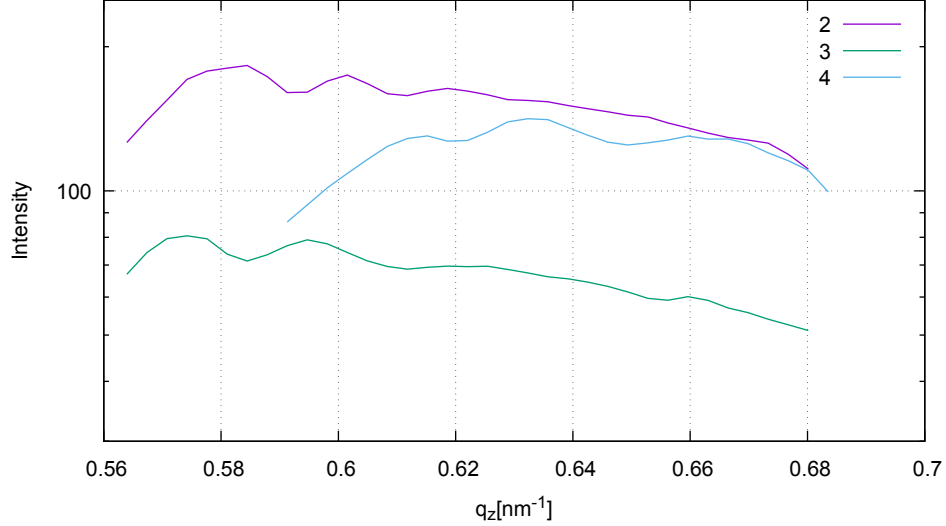


Figure 27: Vertical cuts for samples 2-4 near Yoneda peak

Fitting procedure was also performed in this case. Maximum in the middle was chosen as the reference one, Δq values were calculated with respect to its position. The following average values for spacing were obtained (using formula $\pi/\Delta q$): $d_2 = 138,5 \text{ nm}$, $d_3 = 137,5 \text{ nm}$, $d_4 = 116,6 \text{ nm}$. These values are in quite good agreement with nominal values for large nanowires. For the case of small ones, diameter is overestimated. All differences might be caused by fitting errors, since maxima are quite significantly broadened and not well pronounced.

4 Summary

All the performed studies proved, that obtaining transparent and conductive silver nanowire thin films is possible with the use of airbrush spray-deposition method. The properties of the samples strictly depends on deposition parameters, what was investigated in details. This research enabled to estimate an optimal set o parameters. Transparency of the samples is related linearly to surface coverage. Thickness of the nanowires remained unknown after the initial characterization of the samples, since AFM and optical microscopy did not provide any unequivocal result.

GISAXS patterns were recorded for a series of four nanowire thin film samples. Analysis of the collected data showed, that nanowires have sizes very similar to the information provided by the producer. Results obtained from horizontal cuts fitting are

not consistent with the other findings, what might be related to the fact, that in the model cylinders are assumed to be positioned vertically, not horizontally. Comparison of GISAXS pattern proved, that surface coverage has big influence on the intensity of scattered radiation.

To summarize, all the performed measurements enabled to perform complex studies of morphology and properties of silver nanowire thin films. Complemented with investigation of deposition process, this work is a good starting point for further studies on this kind of structures. The next step will be to perform similar research with layers consisting of aligned nanowires, which were already obtained by the use of grazing incidence spray-coating.

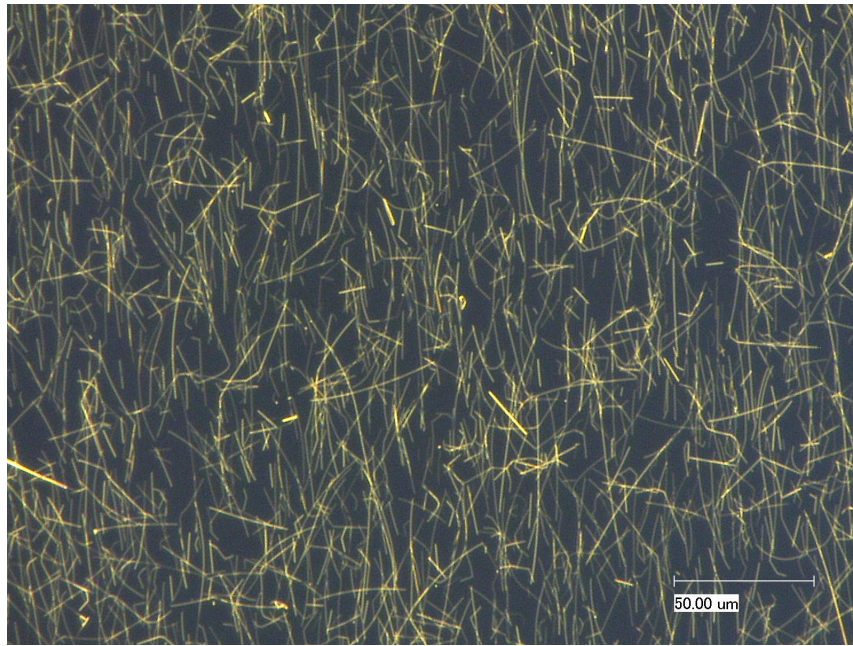


Figure 28: Alignment of nanowires achieved by GI spraying

References

- [1] Stephan V. Roth, *A deep look into the spray coating process in real-time - the crucial role of x-rays*, J. Phys.: Condens. Matter 28, 403003 (2016)
- [2] Herrmann M. 2006 CTR summer program pp 1122
(<http://web.stanford.edu/group/ctr/SummerProgram/TwoPhaseTutorial.pdf>)
- [3] G. Renauda, R. Lazzari, F. Leroy, *Probing surface and interface morphology with Grazing Incidence Small Angle X-Ray Scattering*, Surface Science Reports 64 (2009) 255-380
- [4] G. Herzog, G. Benecke, A. Buffet, B. Heidmann, J. Perlich, J. F. H. Risch, G. Santoro, M. Schwartzkopf, Shun Yu, W. Wurth, S. V. Roth, *In Situ Grazing Incidence Small-Angle X-ray Scattering Investigation of Polystyrene Nanoparticle Spray Deposition onto Silicon*, Langmuir 2013, 29, 1126011266
- [5] I. Horcas et al., Rev. Sci. Instrum. 78, 013705 (2007)
- [6] http://photon-science.desy.de/facilities/petra_iii/beamlines/p03_minaxs/index_eng.html
- [7] Benecke, G. et al., *A customizable software for fast reduction and analysis of large X-ray scattering data sets: applications of the new DPDAK package to small angle X-ray scattering and grazing-incidence small angle X-ray scattering*, J. Appl. Cryst. 47, 1797-1803, (2014)
- [8] A. Buffet, M. M. Abul Kashem, J. Perlich, G. Herzog, M. Schwartzkopf, R. Gehrke, S. V. Roth, *Stripe-Like Pattern Formation in Airbrush-Spray Deposition of Colloidal Polymer Film* Advanced Engineering Materials 2010, 12, No. 12
- [9] P. Zhang, G. Santoro, Shun Yu, S. K. Vayalil, S. Bommel, S. V. Roth, *Manipulating the Assembly of Spray-Deposited Nanocolloids: In Situ Study and Monolayer Film Preparation*, Langmuir 2016, 32, 42514258